Hindawi Publishing Corporation
EURASIP Journal on Wireless Communications and Networking
Volume 2008, Article ID 195948, 14 pages
doi:10.1155/2008/195948

Research Article

Identification of LOS in Time-Varying, Frequency Selective Radio Channels

Serhan Yarkan and Hüseyin Arslan

Department of Electrical Engineering, University of South Florida, 4202 E. Fowler Avenue, ENB-118, Tampa, FL 33620, USA

Correspondence should be addressed to Serhan Yarkan, syarkan@mail.usf.edu

Received 16 August 2007; Revised 15 December 2007; Accepted 22 February 2008

Recommended by Chia-Chin Chong

A method is proposed to identify the existence of line-of-sight (LOS) for time-varying, frequency selective radio channels. The proposed method considers the second-order statistical characteristics of underlying process in the channel taps. Identification is established by comparing the autocorrelation coefficients of the first tap with those of any other tap when the other tap reaches its coherence time. Numerical results and related discussions are presented considering several practical scenarios.

Copyright © 2008 S. Yarkan and H. Arslan. This is an open access article distributed under the Creative Commons Attribution License, which permits unrestricted use, distribution, and reproduction in any medium, provided the original work is properly cited.

1. INTRODUCTION

One of the most important properties of propagation channels for wireless communications is the presence of line-of-sight (LOS) between the transmitter and receiver. Having LOS affects some of the crucial parameters of both the transmission system design and the applications. Transmission frequency (or wavelength) is one of the parameters exemplifying the impact of LOS on the system design. Radio transmissions over millimeter waves (above 10 GHz) require LOS, whereas LOS is not necessary in microwave bands. This stems from the fact that significant transmission losses occur while millimeter waves travel through environment. In millimeter wave bands, atmospheric absorption caused by gases and water vapor leads to very high signal attenuation. Similarly, rain drops cause scattering since the size of drops are on the order of millimeters. Apart from that, foliage losses are also very significant for millimeter wave bands. In addition, it is known that diffusion provides less power at the receiver than specular reflected power and shorter wavelengths suffer from greater diffusion compared to longer wavelengths [1]. Considering all these aspects together, special standards are established for LOS transmission such as 10–66 GHz portion of the physical layer part of IEEE 802.16. Another design parameter on which LOS has a considerable impact is the transmission bandwidth of the system. Measurements show that power delay profiles (PDPs) of ultrawide band (UWB) transmission are affected drastically by the presence/absence of LOS compared to those of non-UWB systems [2–4].

Ranging and positioning are two prominent examples of wireless communication applications on which LOS has significant effects. Currently, there are numerous ranging and positioning applications such as enhanced 911 emergency calling systems (E-911) [5], criminal tracking, and lost-patient locators [6]. In ranging and positioning applications, it is extremely important to know the status of the multipaths received at the receiver. Assume that there is LOS between transmitter and receiver and this is identified by the ranging system of interest. Since the system knows that LOS exists, the time-of-arrival (ToA) estimate can easily be employed in calculating the distance between transmitter and receiver by simply multiplying the speed of the wave used (in radio transmission, of course, it is assumed to be speed of light, $c = 3 \times 10^8$ m/s) with it. However, this is not true for non-line-of-sight (NLOS) cases, since there is no direct path between transmitter and receiver. Therefore, ToA estimates introduce estimation bias into the calculations under NLOS [7]. Moreover, knowledge of being in LOS determines also the method to be used in estimating ToA. Maximum likelihood-based estimators are employed for LOS cases, whereas maximum a posteriori-based estimators are employed for NLOS cases. Note that maximum a posteriori-based estimators are computationally more complex than

maximum likelihood-based estimators. Hence, indirectly, LOS status of the transmission has an impact on the ranging and positioning applications [8].

In conjunction with ranging and positioning, knowledge of being in LOS or NLOS can be used in adjusting some parameters of wireless networks as well. For instance, some specific types of networks such as ad hoc networks, need the geometric characteristics of the environment to improve their communication performances. Due to their dynamic structures, determining the ranges between network nodes as accurately as possible is extremely important to optimize the routing scheme. This is known as "location awareness" [9].

Since identification of LOS provides wireless networks with some sort of awareness, it is worth mentioning a recently emerging technology which depends heavily on "awareness": cognitive radio. Cognitive radio is defined as an adaptive radio system that can sense, be aware of its surrounding environment, and change the transmission parameters according to its observations and past "experiences" [10]. Having these capabilities in hand, a cognitive device that can identify the LOS status of the transmission can easily switch to a higher-order modulation, or even to a higher frequency band to obtain more data rate [11]. In parallel to transmission parameter adaptation for cognitive radio [12], cognitive positioning systems also benefit from LOS status of the transmission in terms of accuracy adaptation that they provide [13].

Due to mutually exclusive relationship between LOS and NLOS, the identification procedure is generally regarded as a composite hypothesis test in which ToA information and ranging measurements are employed [8, 14–16]. Considering that fading channel amplitudes of narrowband systems exhibit Ricean distribution under LOS transmission, the comparison of the theoretical distribution with the observed one gives an idea about LOS/NLOS status of the transmission [17]. Hypothesis testing based on distribution comparison for LOS/NLOS identification has several drawbacks in terms of time consumption and computational complexity. In order to make a reliable decision, a priori knowledge of the noise level of the system is essential [8]. Another method that, again, depends on the comparison of the probability distributions is examining the samples of the first tap [18]. This method has the following main drawbacks: (a) in order to obtain a reliable statistics about the distribution, observing time must be long enough; (b) the transmissions that have relatively weaker LOS component cannot be easily distinguished from other theoretical distributions like Rayleigh fading, which leads to misdetections. (To compare the statistics obtained to a reference, one is accomplished by statistical tests, such as Pearson's test statistics [18] or Kolmogorov-Smirnov test [19].) In order to compensate for the drawback mentioned in (a), the use of estimation of Ricean factor (K) has been proposed [18]. After estimating K, depending on the value estimated, say $\widetilde{K}$, the LOS status is weighted according to a predetermined scale. The predetermined scale is defined over $\mathbb{R}$ and has three sections separated from each other by two K levels, say $K_{\min}$ and $K_{\max}$, which depend on the noise level of the system. Any $\widetilde{K}$ lower than $K_{\min}$, namely, $\widetilde{K} \in (-\infty, K_{\min})$, is regarded as Rayleigh fading (or, in other words, NLOS); any $\widetilde{K}$ greater than $K_{\max}$, namely, $\widetilde{K} \in (K_{\max}, \infty)$, is regarded as obvious Ricean (or, in other words, LOS); for the values in between, namely, for $\widetilde{K} \in [K_{\min}, K_{\max}]$, a linearly changing probability value that depends on the distance to the border, $K_{\min}$ is assigned to the status. It is obvious that this method requires the estimation of Ricean factor (K).

In this study, a method is proposed to identify LOS for time-varying, frequency selective radio channels for coherent receivers. Given that channel and delay acquisition estimations are provided by means of coherent reception algorithms [20–24], LOS identification is performed by comparing second-order statistical characteristics of underlying processes in channel taps. Assuming that the LOS path is in the first tap, a comparison is established via coherence time and by investigating the relationship between underlying processes forming the channel taps. The contributions of this work can be listed as follows:

(C1) It is shown that in the presence of LOS, for a time-varying, frequency selective radio channel, there is a lower bound of K for which the autocorrelation coefficient of the first tap is always greater than those of subsequent taps when they reach their coherence time.

(C2) Based on the proposition above, a LOS identification method is proposed and evaluated under practical scenarios.

Rest of the paper is organized as follows. Section 2.1 introduces the channel model to be used and its second-order statistical properties. Section 2.2 provides a theoretical lower bound of K for LOS identification in conjunction with coherence time. In Section 2.3, a method is proposed to identify LOS based on the lower bound found in Section 2.2. Section 3 presents the numerical results considering both theoretical and practical cases. In Section 4, concluding remarks are given including UWB transmission.

2. THE PROPOSED APPROACH

2.1. The channel model

Time-varying, frequency selective radio channels can be represented at baseband in the form of

$$h(t,\tau) = \sum_{k=0}^{L-1} h_k(t)\delta(\tau - \tau_k(t)), \tag{1}$$

where L is the total number of multipaths, $h_k(t)$ denotes the complex, time-varying path gain corresponding to kth multipath, $\delta(\cdot)$ is the Dirac delta function, τ denotes the delay axis, and $\tau_k(t)$ denotes the path-arrival times [25]. At a time instant t, kth channel tap gain $h_k(t)$ is obtained by sum of a diffuse component and a specular component as follows [26]:

$$h_k(t) = s_k(t) + d_k(t), \tag{2}$$

where

$$s_k(t) = \sigma_{s_k} e^{j(\omega_D \cos(\theta_0^{(k)})t + \phi_0^{(k)})}, \tag{3a}$$

$$d_k(t) = \sigma_{d_k} \frac{1}{\sqrt{M_k}} \sum_{m=1}^{M_k} b_m e^{j(\omega_D \cos(\theta_m^{(k)})t + \phi_m^{(k)})}. \tag{3b}$$

In (3a), σ_{s_k} denotes the magnitude of the specular component, $j = \sqrt{-1}$, ω_D is the maximum Doppler frequency in radian, $\theta_0^{(k)}$ is the angle-of-arrival (AoA), and $\phi_0^{(k)}$ is the phase shift for $s_k(t)$. (Even though $\theta_0^{(k)}$ and $\phi_0^{(k)}$ belong to specular component in kth tap, in actual propagation environments, it is very unlikely to have a strong specular component in each tap. However, there are some cases in which there is specular component in both the first and second taps. Nevertheless, as will be discussed in this section subsequently, this can still be treated with the aid of the concept of "underlying process.") Here, ω_D is equal to $(2\pi f_c v/c)$, where f_c is the transmission frequency, v represents speed of the mobile, and c is speed of the propagation. In (3b), σ_{d_k} denotes the magnitude of the diffused component, M_k represents the number of incoming waves, b_m is the amplitude, and $\phi_m^{(k)}$ is the phase shift for mth diffused component coming with the angle $\theta_m^{(k)}$, respectively. (In the literature, instead of speaking of individual statistics of b_ms, generally, the statistics of their superposition is discussed. For instance, when narrowband channels are considered, central limit theorem is generally applied when $M_k \to \infty$ leading to a Rayleigh amplitude distribution for kth tap in the absence of LOS.) However, it must be stated that in the method proposed, there is only one condition for (3b): $M_k \geq 1$. This is essential, because when $M_k = 0$, $d_k(t)$ does not exist. However, the method proposed is not limited to any other condition such as narrow-band channels, $M_k \to \infty$, or uniformly distributed $\theta_m^{(k)}$.

For the sake of completeness, the characteristics of path-arrival times, namely, $\tau_k(t)$, can be investigated. Since multipath effect is caused by objects in the surrounding environment, it can be concluded that path-arrival times are affected by the locations of these objects. Assuming that the surrounding objects within an environment are randomly located, the path arrival statistics can be considered as Poisson process as suggested in [27]. However, the assumption that allows for randomly located objects might not be valid for urban environments, since the residential areas and buildings in urban environments have some sort of geometric structures rather than random, irregular structures. Hence, path-arrival times need to be modeled in a different manner in order for the model to be realistic. One of the very well-known models for path-arrival times is known as modified Poisson process [28]. Note that, $\tau_0(t)$ is deterministic rather than random in LOS cases, due to the distance-delay relationship in ranging and positioning applications mentioned earlier in Section 1.

When the autocorrelation function of (2) is considered assuming that uncorrelated scattering is satisfied (i.e., uncorrelated attenuation and phase shift with paths of different delays exist) and the specular and diffused components are independent, the autocorrelation of kth tap can be calculated as

$$\begin{aligned} R_{h_k}(\Delta t) &= E\{h_k(t)h_k^*(t+\Delta t)\} \\ &= E\{(s_k(t)+d_k(t))(s_k(t+\Delta t)+d_k(t+\Delta t))^*\} \\ &= R_{s_k}(\Delta t) + R_{d_k}(\Delta t), \end{aligned} \tag{4}$$

where $E\{\cdot\}$ is the expected value operator and $(\cdot)^*$ represents the complex conjugate of its argument. For the sake of brevity, autocorrelation *coefficients* can be used in analysis instead of autocorrelation values. Autocorrelation coefficients are obtained as follows:

$$\rho_x(\Delta t) = \frac{R_x(\Delta t)}{R_x(0)} \tag{5}$$

for any random process $x(t)$. Since the specular and diffused components are previously assumed to be independent of each other, then, (4) can be reorganized in terms of autocorrelation coefficients as follows:

$$\begin{aligned} \rho_{h_k}(\Delta t) &= \frac{R_{h_k}(\Delta t)}{R_{h_k}(0)} = \frac{R_{s_k}(\Delta t) + R_{d_k}(\Delta t)}{\sigma_{s_k}^2 + \sigma_{d_k}^2} \\ &= \frac{K_k}{K_k+1}\rho_{s_k}(\Delta t) + \frac{1}{K_k+1}\rho_{d_k}(\Delta t), \end{aligned} \tag{6}$$

where $K_k = \sigma_{s_k}^2/\sigma_{d_k}^2$, which defines the power ratio between specular and diffused components and is known as Ricean factor. In the rest of the paper, the subscript k is dropped from K_k for the sake of brevity. Hence, from this point on when K is used, it must be understood that the Ricean factor for kth tap is referred unless otherwise stated.

2.2. Bound for K parameter

Note that (6) is a complex-valued function in general. Therefore, the squared-envelope of (6) can be calculated as well:

$$\begin{aligned} |\rho_{h_k}(\Delta t)|^2 &= (\rho_{h_k}(\Delta t)\rho_{h_k}^*(\Delta t)) \\ &= \left(\frac{K}{K+1}\right)^2 |\rho_{s_k}(\Delta t)|^2 + \frac{2K\Re(\rho_{s_k}(\Delta t)\rho_{d_k}^*(\Delta t))}{(K+1)^2} \\ &\quad + \left(\frac{1}{K+1}\right)^2 |\rho_{d_k}(\Delta t)|^2, \end{aligned} \tag{7}$$

where $\Re(\cdot)$ denotes the real part of its argument.

In (7), $|\rho_{s_k}(\Delta t)|^2$ becomes unity in connection with (3a) and (5). After some mathematical manipulations (7) can be

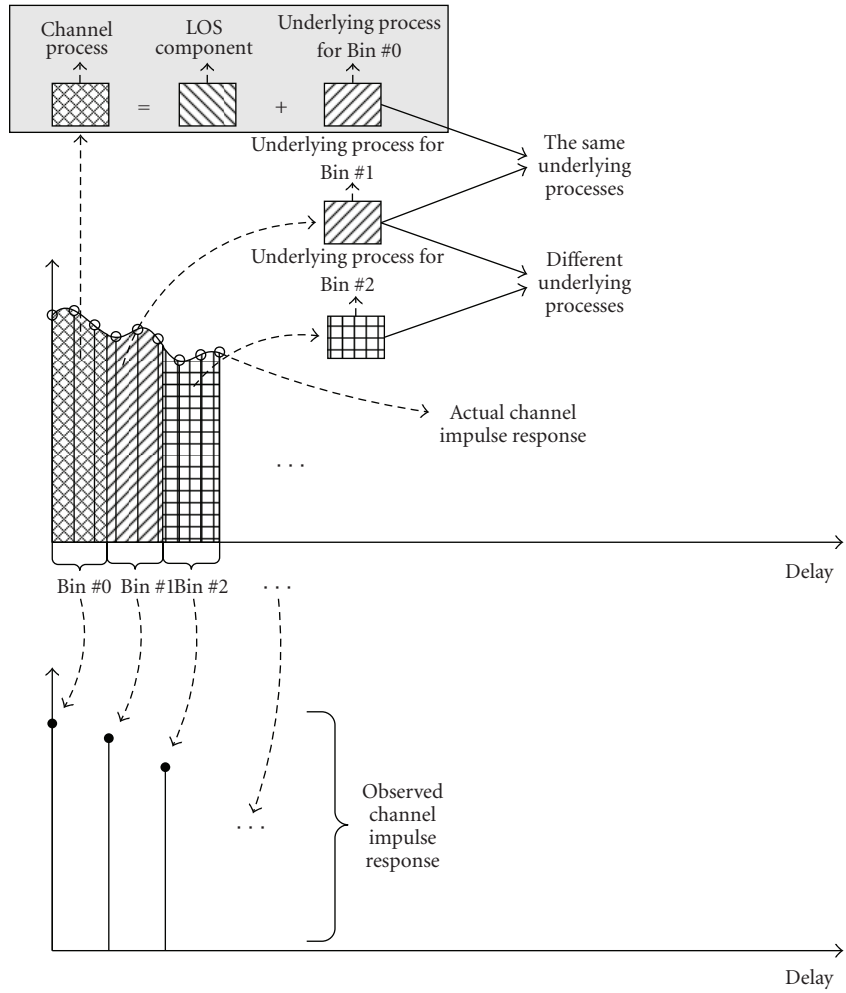

Figure 1: Illustration of the concept of "underlying process" and its relationship with channel impulse response. In this figure, first bin consists of two processes. One of them, which is referred to as "Underlying process for Bin ♯0," is the same as the process of "Bin ♯1." However, underlying processes for Bin ♯1 and ♯2 are not the same.

rewritten in the following form in order to have an easier analysis in further steps:

$$\begin{aligned}&\left|\rho_{h_k}(\Delta t)\right|^2\\&\quad=\left(\frac{K}{K+1}\right)^2+\frac{2K\left|\rho_{d_k}(\Delta t)\right|\cos\left(\omega_D\cos\left(\theta_0^{(k)}\right)\Delta t+\Psi(\Delta t)\right)}{(K+1)^2}\\&\qquad+\left(\frac{1}{K+1}\right)^2\left|\rho_{d_k}(\Delta t)\right|^2,\end{aligned}\tag{8}$$

where

$$\Psi(\Delta t)=\arccos\left(\frac{\Re\left(\rho_{d_k}(\Delta t)\right)}{\left|\rho_{d_k}(\Delta t)\right|}\right).\tag{9}$$

Note that (8) is composed of two parts: the part which is solely a function of K (the first term to the right of equality in (8)) and the part which is a function of $|\rho_{d_k}(\Delta t)|$ (last two terms to the right of equality in (8)). From this perspective, $|\rho_{d_k}(\Delta t)|$ actually corresponds to the *underlying process* part of $|\rho_{h_k}(\Delta t)|$. An illustration of the concept of underlying processes including their relationship with the tapped delay line model is shown in Figure 1. Width of bins represents the resolution of the receiver over delay axis. Assume that a receiver is capable of operating on infinite transmission bandwidth. This receiver can distinguish each multipath delay, since the width of bins converges to zero. However, in reality, no receiver is capable of operating on infinite transmission bandwidth. Therefore, in reality, receivers "see" sum of multipaths falling into the same bin leading to multipath fading channel as shown in Figure 1. Hence, the model in (1) represents the observed channel. Comparing UWB receivers with traditional narrowband receivers sheds light on this situation. In narrowband channels fading channel amplitudes can be modeled as Rayleigh (or depending on having a dominant specular component, Ricean) process. However, this does not hold for UWB, since the time resolution of the UWB receiver (i.e., width of bins) is extremely small

compared to that for narrowband systems. Therefore, even though there might be many distinct multipaths present, due to the limited capability of the receiver, "observed channel" consists of superimposed multipath components falling into the same bin. Currently, channel estimation is an essential part of coherent receivers. Receivers observe the channel through the use of several channel estimation techniques.

Peculiar to LOS scenarios, first bin includes the LOS component beside some other paths which form the diffused component defined in (3b). Therefore, in LOS scenarios, h_0 corresponds to the tap ($k = 0$) that contains LOS component. When the taps are considered for $\bar{k}$ which defined as the set of subsequent taps (i.e., $\bar{k} = \{k \mid k > 0\}$), the LOS component will not be present anymore. However, some measurements show that for $\bar{k}$, there may still be a relatively weaker specular component compared to the first tap [29]. Nevertheless, as will be explained in the subsequent sections, having such a component causes to have different underlying processes for the subsequent taps ($\bar{k}$); but, it can still be treated with the method proposed. Despite it is out of the scope of this study, it is worth mentioning the impact of UWB transmission on the concept of underlying process as well. Since the increase in transmission bandwidth leads to a finer resolution in time, the width of the bins shrinks. This clearly affects the concept of underlying process, since the receiver is able to distinguish each individual path. Hence, it might not be possible for the receiver to have both specular and diffused component simultaneously within the same bin or tap. Identification of LOS in UWB cases will be discussed in Section 4.

Before proceeding into further details of the method proposed, it is appropriate to give the definition of coherence time of a channel.

Definition 1 (coherence time of a channel [25]). "Coherence time is the time duration over which two received signals have a strong potential for amplitude correlation." For practical purposes, the coherence time can be defined as the time duration over which the autocorrelation coefficients are above 0.5.

In order to establish the connection between LOS identification and statistics of the channel process, the following proposition is defined.

Proposition 1. *In a time-varying, frequency selective radio channel, if the first channel tap contains a specular component with $K > 3$, it will always have a higher autocorrelation coefficient compared to that of any one of the subsequent taps at the moment where any one of the subsequent taps reaches its coherence time.*

Proposition 1 includes at least two taps and their autocorrelation coefficients. Therefore, it is appropriate to consider the statistical characteristics of the processes that form these taps. In (8), in terms of underlying processes, there are only two possibilities for the channel that contains both specular and diffused components. The temporal statistics of the underlying process of h_k, namely, $|\rho_{d_k}(\Delta t)|$, can be in either of the following cases.

Case 1. The same in each tap.

Case 2. Different in each tap (or in some of the taps as illustrated in Figure 1).

In fact, Case 1 is a special case of Case 2. In order to see this relationship, assume that one of the subsequent taps $\bar{k}$ reaches its coherence time at Δt_1, that is, $|\rho_{h_{\bar{k}}}(\Delta t_1)| = 0.5$. Let the difference between the autocorrelation coefficients of underlying processes, namely, $|\rho_{d_0}(\Delta t_1)|$ and $|\rho_{d_{\bar{k}}}(\Delta t_1)|$, be defined in terms of $e(\Delta t_1)$ in a general way as follows:

$$\left|\rho_{d_0}(\Delta t_1)\right| = \left|\rho_{d_{\bar{k}}}(\Delta t_1)\right| \pm e(\Delta t_1). \tag{10}$$

In (10), note that Case 2 is identical to Case 1 for $e(\Delta t_1) = 0$. Note also that since $0 \le |\rho_x(\Delta t_1)| \le 1$ for any random process $x(t)$, Definition 1 requires $e(\Delta t_1) \in [0, 0.5)$ in light of (10). Therefore, proving solely Case 2 will be sufficient to investigate Proposition 1. However, due to the sign of difference term in (10), Case 2 can be broken into two parts for Δt_1 as follows:

$$\text{Case 2} := \begin{cases} \left|\rho_{d_{\bar{k}}}(\Delta t_1)\right| - e(\Delta t_1), & \text{Case 2(a)}, \\ \left|\rho_{d_{\bar{k}}}(\Delta t_1)\right| + e(\Delta t_1), & \text{Case 2(b)}, \end{cases} \tag{11}$$

Note that in (11), $e(\Delta t_1)$ is considered as an additive term. One might ask why $e(\Delta t_1)$ is modeled as an additive term instead of a multiplicative term. There are analytical reasons for $e(\Delta t_1)$ to be chosen as additive. First and foremost, multiplication is a special case of multiple addition. Second, if $e(\Delta t_1)$ were to be chosen as a multiplicative term, the result would not change; however, because of the scaling factor, the domain of $e(\Delta t_1)$ would be different. Bearing in mind that $|\rho_{d_0}(\Delta t_1)|$ and $|\rho_{d_{\bar{k}}}(\Delta t_1)|$ are defined as $0 \le |\rho_{d_0}(\Delta t_1)|, |\rho_{d_{\bar{k}}}(\Delta t_1)| \le 1$, and $|\rho_{d_0}(\Delta t_1)| = e(\Delta t_1)|\rho_{d_{\bar{k}}}(\Delta t_1)|$; it can be concluded that $e(\Delta t_1) \in [0, 2]$ because of Definition 1 ($|\rho_{d_{\bar{k}}}(\Delta t_1)| = 0.5$). Note that the interval $[0, 1)$ corresponds to Case 2(a) since $|\rho_{d_0}(\Delta t_1)| < |\rho_{d_{\bar{k}}}(\Delta t_1)|$, whereas the interval $(1, 2]$ corresponds to Case 2(b) since $|\rho_{d_0}(\Delta t_1)| > |\rho_{d_{\bar{k}}}(\Delta t_1)|$. Clearly, Case 1, which is a special case of Case 2, occurs when $e(\Delta t_1) = 1$.

Now, one can proceed to investigate the two possible situations in (11) along with the corresponding proofs for Case 2. Therefore, first, the squared-envelope of autocorrelation coefficients of h_0 and $h_{\bar{k}}$ must be calculated:

$$\begin{aligned} \left|\rho_{h_0}(\Delta t)\right|^2 &= \left(\frac{K_0}{K_0+1}\right)^2 \\ &\quad + \frac{2K_0\left|\rho_{d_0}(\Delta t)\right|\cos\left(\omega_D \cos\left(\theta_0^{(0)}\right)\Delta t + \Psi(\Delta t)\right)}{(K_0+1)^2} \\ &\quad + \left(\frac{1}{K_0+1}\right)^2 \left|\rho_{d_0}(\Delta t)\right|^2, \\ \left|\rho_{h_{\bar{k}}}(\Delta t)\right|^2 &= \left|\rho_{d_{\bar{k}}}(\Delta t)\right|^2. \end{aligned} \tag{12}$$

Now, it will be shown that there is a lower boundary of K_0 (K factor for the first tap) for which h_0 always has a higher autocorrelation coefficient value compared to those of the subsequent taps ($h_{\bar{k}}$) when they reach their coherence time.

Proof of Proposition 1 for Case 2(a). If (11)(Case 2(a)) is embedded into (8) along with $f(\Delta t_1) = \omega_D \cos(\theta_0^{(0)})\Delta t_1 + \Psi(\Delta t_1)$ and $|\rho_{d_{\bar{k}}}(\Delta t_1)| = 0.5$, it yields

$$\begin{aligned}
&|\rho_{h_0}(\Delta t_1)|^2 \\
&= \left(\frac{K_0}{K_0+1}\right)^2 + \frac{2K_0(|\rho_{d_{\bar{k}}}(\Delta t_1)| - e(\Delta t_1))\cos(f(\Delta t_1))}{(K_0+1)^2} \\
&\quad + \left(\frac{|\rho_{d_{\bar{k}}}(\Delta t_1)| - e(\Delta t_1)}{K_0+1}\right)^2 \\
&= \left(\frac{K_0^2 + K_0\cos(f(\Delta t_1)) + 0.25}{(K_0+1)^2}\right) \\
&\quad + \left(\frac{e^2(\Delta t_1) - 2e(\Delta t_1)K_0\cos(f(\Delta t_1)) - e(\Delta t_1)}{(K_0+1)^2}\right).
\end{aligned} \tag{13}$$

If (13) is rewritten, then

$$\begin{aligned}
|\rho_{h_0}(\Delta t_1)|^2 &= \underbrace{\left(\frac{K_0^2 + e^2(\Delta t_1) + 0.25}{(K_0+1)^2}\right)}_{>0 \ \forall K_0, \Delta t_1} \\
&\quad + \left(\frac{K_0\cos(f(\Delta t_1))(1 - 2e(\Delta t_1)) - e(\Delta t_1)}{(K_0+1)^2}\right).
\end{aligned} \tag{14}$$

Recall that it is assumed that $\bar{k}$th tap reaches its coherence time at Δt_1 (i.e., $|\rho_{d_{\bar{k}}}(\Delta t_1)| = 0.5$). In this case, the lowest value of (14) for that specific Δt_1 is obtained if

$$\omega_D \cos(\theta_0^{(0)})\Delta t_1 + \Psi(\Delta t_1) = (2l+1)\pi \tag{15}$$

is satisfied, where $l \in \mathbb{Z}^+$, since $e(\Delta t_1) \in (0, 0.5)$ and the first term in (14) is positive for all Δt_1 and K_0 values. (Here, note that $e(\Delta t_1)$ is defined within the open interval $(0, 0.5)$, although it is $e(\Delta t_1) \in [0, 0.5)$ in (10). This is because (10) refers to the general case including both Cases 1 and 2, whereas the proof considers only Case 2, which excludes $e(\Delta t_1) = 0$.) Therefore, it can be reorganized to yield the following:

$$\begin{aligned}
&|\rho_{h_0}(\Delta t_1)|^2 \\
&= \left(\frac{K_0^2 - K_0 + 0.25}{(K_0+1)^2}\right) + \left(\frac{e^2(\Delta t_1) + 2e(\Delta t_1)K_0 - e(\Delta t_1)}{(K_0+1)^2}\right) \\
&= \frac{(K_0 - 0.5)^2}{(K_0+1)^2} + \frac{e^2(\Delta t_1) + (2K_0 - 1)e(\Delta t_1)}{(K_0+1)^2}.
\end{aligned} \tag{16}$$

If a change of variable is applied with $(K_0 - 0.5) = u$, then

$$|\rho_{h_0}(\Delta t_1)|^2 = \underbrace{\left(\frac{u + e(\Delta t_1)}{u + 3/2}\right)^2}_{\mathcal{M}_1} \tag{17}$$

is obtained. Since the condition $|\rho_{h_{\bar{k}}}(\Delta t_1)| < |\rho_{h_0}(\Delta t_1)|$ (or equivalently $|\rho_{h_{\bar{k}}}(\Delta t_1)|^2 < |\rho_{h_0}(\Delta t_1)|^2$) is investigated,

$$\begin{aligned}
|\rho_{h_{\bar{k}}}(\Delta t_1)| &< \left(\frac{u + e(\Delta t_1)}{u + 3/2}\right), \\
0.5 &< \left(\frac{u + e(\Delta t_1)}{u + 3/2}\right), \\
\frac{3}{2} - 2e(\Delta t_1) &< u
\end{aligned} \tag{18}$$

are obtained and if the change of variable is applied back while recalling $e(\Delta t_1) \in (0, 0.5)$, then

$$2 < K_0 \tag{19}$$

which completes the first part of the proof of Case 2. □

Proof of Proposition 1 for Case 2(b). Similar to Case 2(a), if (11)(Case 2(b)) is embedded into (8) and the same steps between (13)–(17) are followed, it is found that

$$\mathcal{M}_2 = \left(\frac{u - e(\Delta t_1)}{u + 3/2}\right)^2 \tag{20}$$

which reads

$$3 < K_0. \tag{21}$$

□

Finally, proof of Proposition 1 can be unified, since all possible cases have been examined.

Proof of Proposition 1. Considering (19) and (21) together,

$$K \in ((K_0 > 3) \cap (K_0 > 2)) \equiv K_0 > 3 \tag{22}$$

is obtained and this completes the proof of Proposition 1. □

Note that the worst case condition which is stated in (15) is considered in deriving both (17) and (20). Although theoretically it is possible, in order for the worst case scenario to take its place, several independent parameters must satisfy a unique condition. Assume that all the correlation properties ($|\rho_{h_k}(\Delta t)|$) of underlying processes are the same for each tap (i.e., $e(\Delta t_1) = 0$). For the sake of brevity, assume also that $\rho_{h_k}(\Delta t_1)$ is real. (A very well-known example set of channel models that satisfy these properties can be found in International Telecommunication Union-Radiocommunications (ITU-R) channel models [30].) Therefore, $\Psi(\Delta t_1) = 0$, which yields

$$\begin{aligned}
\omega_D \cos(\theta_0^{(0)})\Delta t_1 &= (2l+1)\pi, \\
\Delta t_1 &= \frac{(2l+1)c}{2f_c v\cos(\theta_0^{(0)})}.
\end{aligned} \tag{23}$$

In (23), because $\theta_0^{(0)}$ and v are two independent parameters, it is very unlikely that the worst case scenario takes its place in practical cases. As will be shown in Section 3, the condition $K_0 > 3$ can be relaxed for most of the practical cases. However, it requires further investigations to see how much relaxation can be allowed in K_0.

2.3. LOS identification

Combining Definition 1 and Proposition 1, identification of LOS can be established by comparing the difference $|\rho_{h_0}(\Delta t_1)|^2 - |\rho_{h_{\bar{k}}}(\Delta t_1)|^2$ with a nonnegative threshold where Δt_1 is the coherence time for $h_{\bar{k}}$, namely, $|\rho_{h_{\bar{k}}}(\Delta t_1)| = 0.5$. In this regard, the identification process can formally be stated as

$$\mathcal{T} := \begin{cases} \text{LOS}, & \text{if } \left(|\rho_{h_0}(\Delta t_1)|^2 - |\rho_{h_{\bar{k}}}(\Delta t_1)|^2\right) > z, \\ \text{NLOS}, & \text{otherwise}, \end{cases} \tag{24}$$

where $\mathcal{T}$ denotes the status of the transmission and z denotes the threshold. Note that if the autocorrelation coefficients are known, in other words, if they can perfectly be estimated, (24) can detect LOS for $K_0 > 3$ with $z = 0$ as shown in (22). However, in practical cases, receiver deals with limited number of channel samples. Moreover, these samples might have errors due to the channel estimation process. Limited number of samples with possible errors forces the receiver to use estimations instead of the actual autocorrelation coefficients. Hence, a nonzero threshold z is required in practical cases. A numerical method is applied in Section 3 in order to obtain a proper value for z.

In this sequel, two issues must be investigated regarding the identification procedure. First, one might want to know what happens when coherence time is reached at different time shifts. More formally, one needs to know whether the identification holds if $|\rho_{h_{\bar{k}}}(\Delta t_2)| = 0.5$, where $\Delta t_1 < \Delta t_2$. As shown in proof of Proposition 1, the identification does not depend on time shifts Δt. Identification holds as long as $|\rho_{h_{\bar{k}}}(\cdot)| = 0.5$ is satisfied, which does not consider when and how many times $|\rho_{h_{\bar{k}}}(\cdot)| = 0.5$ occurs. Second, one might want to know whether it is better to use squared-envelope (i.e., $|\cdot|^2$) instead of magnitude (i.e., $|\cdot|$) notation. From the analysis perspective, there is no difference between using squared-envelopes and magnitudes, because in terms of inequality, for any two arbitrary complex numbers, say c_i and c_j, $(|c_i|^2 > |c_j|^2) \Leftrightarrow (|c_i| > |c_j|)$. However, for complex numbers, squared-envelope is obtained simply by multiplying a complex number with its complex conjugate, whereas magnitude includes one extra square-root operation in addition to complex conjugate multiplication. Squared-envelope notation is preferred regarding this fact.

3. NUMERICAL RESULTS

In order to test the proposed method, several simulations have been performed. Simulations can be categorized as follows: (i) testing the validity of the method proposed for Cases 1 and 2 based on the assumption that channel estimation is perfect; and (ii) testing the performance of the method proposed under practical scenarios. For the category (i), two different Doppler spectrum shapes are considered for the underlying processes: (I) Jakes' (classical) type and (II) GAUS1 type. (The autocorrelation function and Doppler spectrum of a channel are dual of each other via Fourier transform). Therefore, time-varying nature of the channel can be given in either temporal (*coherence time*) or spectral domain (*Doppler spread*). In the literature, generally, time-varying nature of the channel is described by

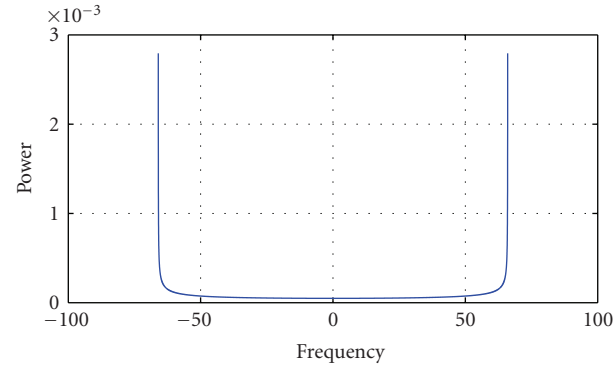

(a) Jakes' type Doppler spectrum

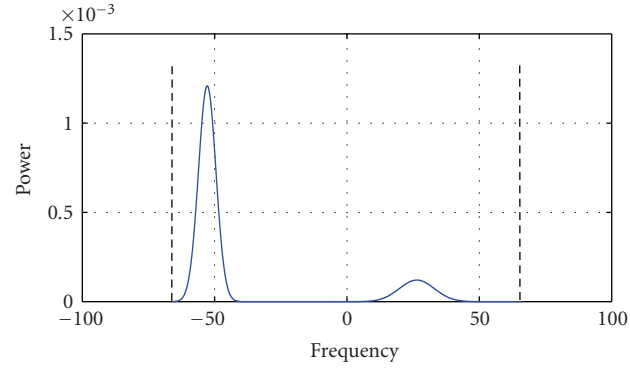

(b) GAUS1 type Doppler spectrum

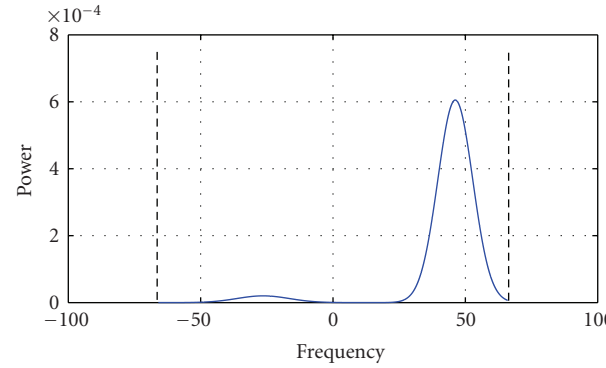

(c) GAUS2 type Doppler spectrum

FIGURE 2: Different Doppler spectra that are encountered in different environments for 900 MHz carrier frequency and a mobile speed of 22 m/s. Vertical dashed lines in Figures 2(b) and 2(c) correspond to maximum Doppler frequency, which is 66 Hz.

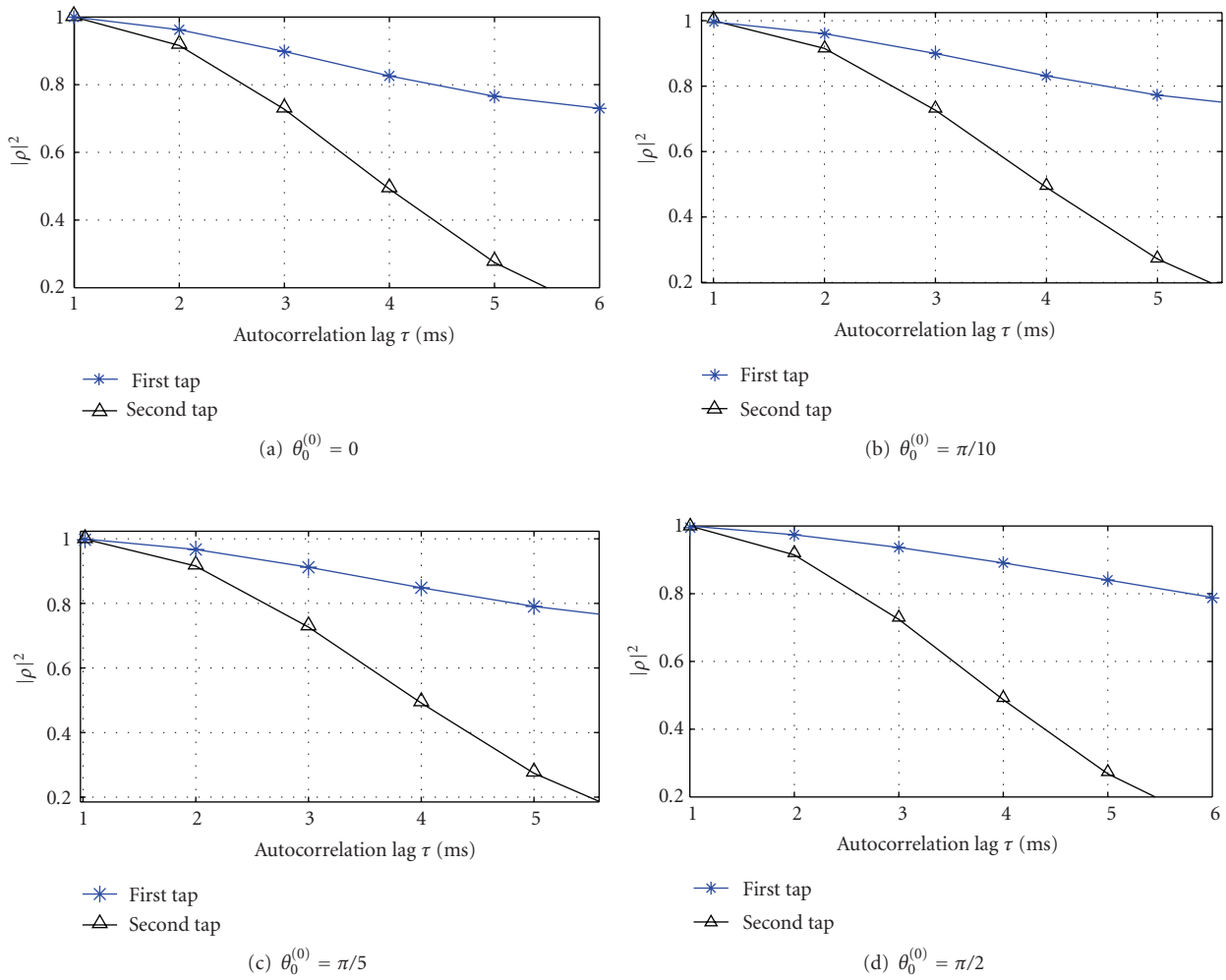

FIGURE 3: Squared-envelope of the autocorrelations of first and second taps for common parameters $K_0 = 10$, $\nu = 20$ m/s, and the set of AoAs $\{\theta_0^{(0)}\}$.

the shape of its Doppler spectrum. Hence, in this section, spectral-domain name convention is adopted to emphasize the characteristics of different underlying processes.) (This Doppler spectrum is one of the four Doppler spectra defined in European Co-operation in the field of Scientific and Technical research (COST) 207. It is the sum of two Gaussian functions (see (25) and (26)). However, it is used for the taps whose delays are in $[0.5\,\mu s, 2\,\mu s]$ [31].) (I) is employed in the majority of the simulation scenarios, since it is very widely used in the literature. However, (II) is used for simulating the cases in which the underlying processes are different. The following two reasons are considered in selecting GAUS1: (R1) GAUS1 type of Doppler spectrum creates one of the most challenging situations for the method proposed, since it forms an underlying process for the subsequent taps ($h_{\bar{k}}$) in which there are two strong distant scatterers; (R2) GAUS1 type of Doppler spectrum causes the autocorrelation function of the tap of interest to be a complex-valued function, whereas (I) yields a real-valued function. Three prominent Doppler spectra including the ones used in the simulations are presented in Figure 2.

Common parameters which are used in simulations are given in Table 1. Note that, in Table 1, the AoAs are only chosen from the interval $[0, \pi/2]$. This is due to the fact that $\cos(\cdot)$ is an even function and there are two nested $\cos(\cdot)$ functions in (8). The following main parameter subset is used for presenting the simulation results: $K_0 = 10$, $\nu = 20$ m/s, $\theta_0^{(0)} = \pi/5$. In addition to this subset, signal-to-noise-ratio (SNR) = 10 dB is employed in presenting the results for the category (ii). Here, noise is complex-valued and assumed to be white and its amplitudes are Gaussian distributed with $\mathcal{N}(0, \sigma_N^2)$. In order to reflect the influence of each parameter, results will be presented by allowing one of the variables to change while keeping the rest fixed.

For the category (i), first Case 1 is considered. In Case 1), the underlying processes are assumed to be the same, that is, of Jakes' type in both first and second taps. The results are presented in Figures 3–5. In Figure 3, the impact of AoA is shown while K_0 and ν are fixed. When $h_{\bar{k}}$ reaches its

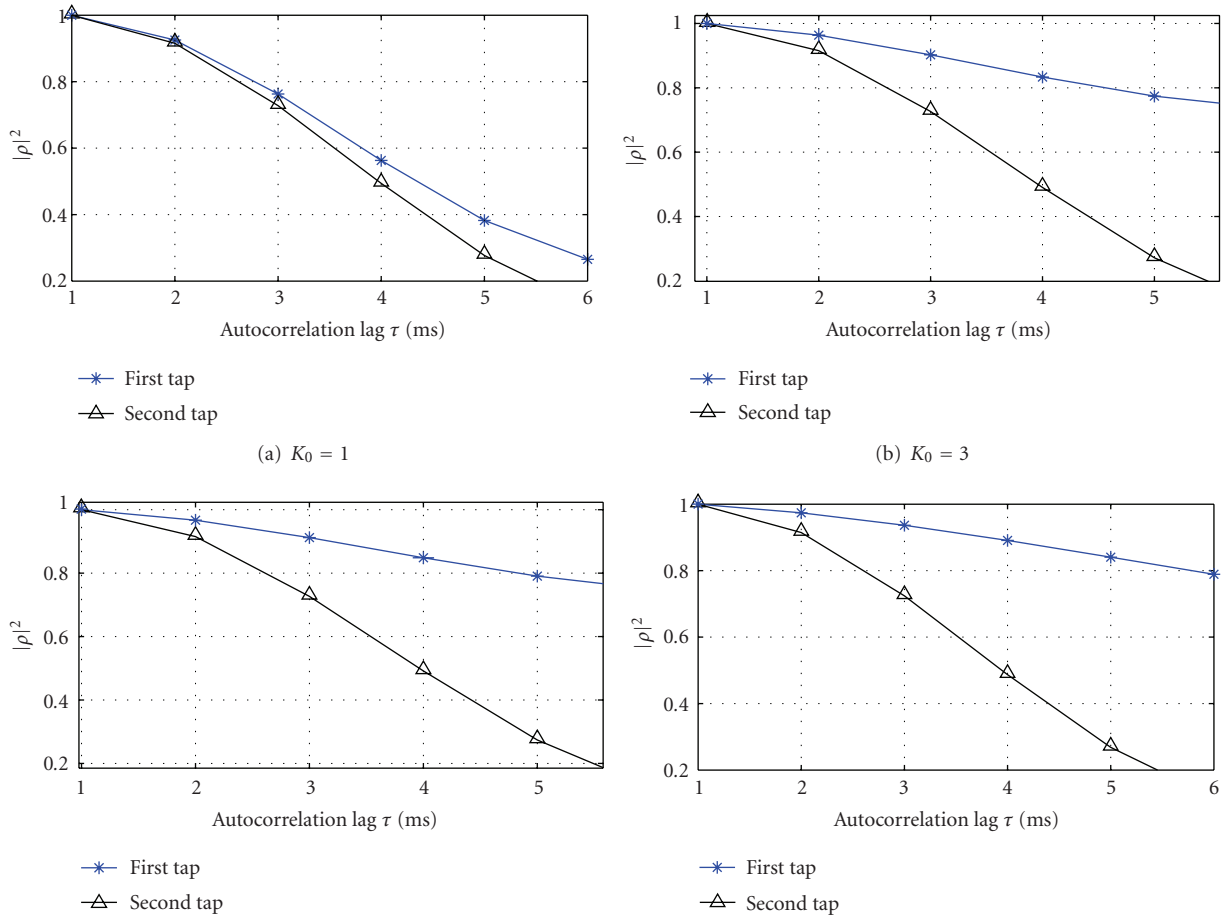

Figure 4: Squared-envelope of the autocorrelations of the first and second taps for common parameters $\theta_0^{(0)} = \pi/5$, $v = 20$ m/s, and the set of $\{K_0\}$.

Table 1: General parameter set for the simulations.

Simulation parameter	Values used
Transmission frequency (f_c):	900 MHz
Mobile speed (v):	$\{1, 3, 10, 20\}$ m/s
Channel sampling frequency (f_s):	1 KHz
AoA ($\theta_0^{(0)}$):	$\{0, \pi/10, \pi/5, \pi/2\}$ radian
K_0 values:	$\{1, 3, 5, 10\}$

coherence time, that is $|\rho_{h_{\bar{k}}}(\Delta t_1)| = 0.5$ (or equivalently $|\rho_{h_{\bar{k}}}(\Delta t_1)|^2 = 0.25$), the difference between $|\rho_{h_0}(\Delta t_1)|^2$ and $|\rho_{h_{\bar{k}}}(\Delta t_1)|^2$ is significant for all values of AoA. Therefore, it can be concluded that the impact of AoA, namely, $\theta_0^{(0)}$, is not significant for the method proposed.

In order to evaluate the impact of K_0, Figure 4 can be investigated. It is seen that the difference between $|\rho_{h_0}(\Delta t_1)|^2$ and $|\rho_{h_{\bar{k}}}(\Delta t_1)|^2$ is very significant in Figures 4(b), 4(c), and 4(d), as expected because of Proposition 1. However, this difference is insignificant in Figure 4(a) compared to the cases where $K_0 > 3$.

Similar to $\{\theta_0^{(0)}\}$ and $\{K_0\}$ sets, Figure 5 can be investigated to determine the impact of set $\{v\}$ upon the method proposed. In Figure 5(a), it is seen that when speed of the mobile is close to zero, the difference between $|\rho_{h_0}(\Delta t_1)|^2$ and $|\rho_{h_{\bar{k}}}(\Delta t_1)|^2$ is not significant. However, as v increases, the difference between $|\rho_{h_0}(\Delta t_1)|^2$ and $|\rho_{h_{\bar{k}}}(\Delta t_1)|^2$ increases drastically as can be seen in Figures 5(b), 5(c), and 5(d). This drastic effect of v can be explained in the following way. For $v = 0$, the channel taps become time-invariant according to (3a) and (3b). Since the channel taps do not change in time, their autocorrelation coefficients become unified. This implies that the difference which is used in LOS identification gets weaker while $v \to 0$ and totally vanishes at $v = 0$ (i.e., "time-invariant channel"). Conversely, for $v > 0$, the autocorrelation coefficients of the channels will differ as shown in Figure 5. Note also that the effect of v is independent of any type of Doppler spectrum, because shape of the spectrum is determined by AoAs not by v.

In this sequel, it will be useful to see the cases when $K_0 \in (0, 3)$. In order to investigate this, Case 1 is considered along with (I), since it is very widely used in wireless mobile radio channel models. In these simulations, all the parameter

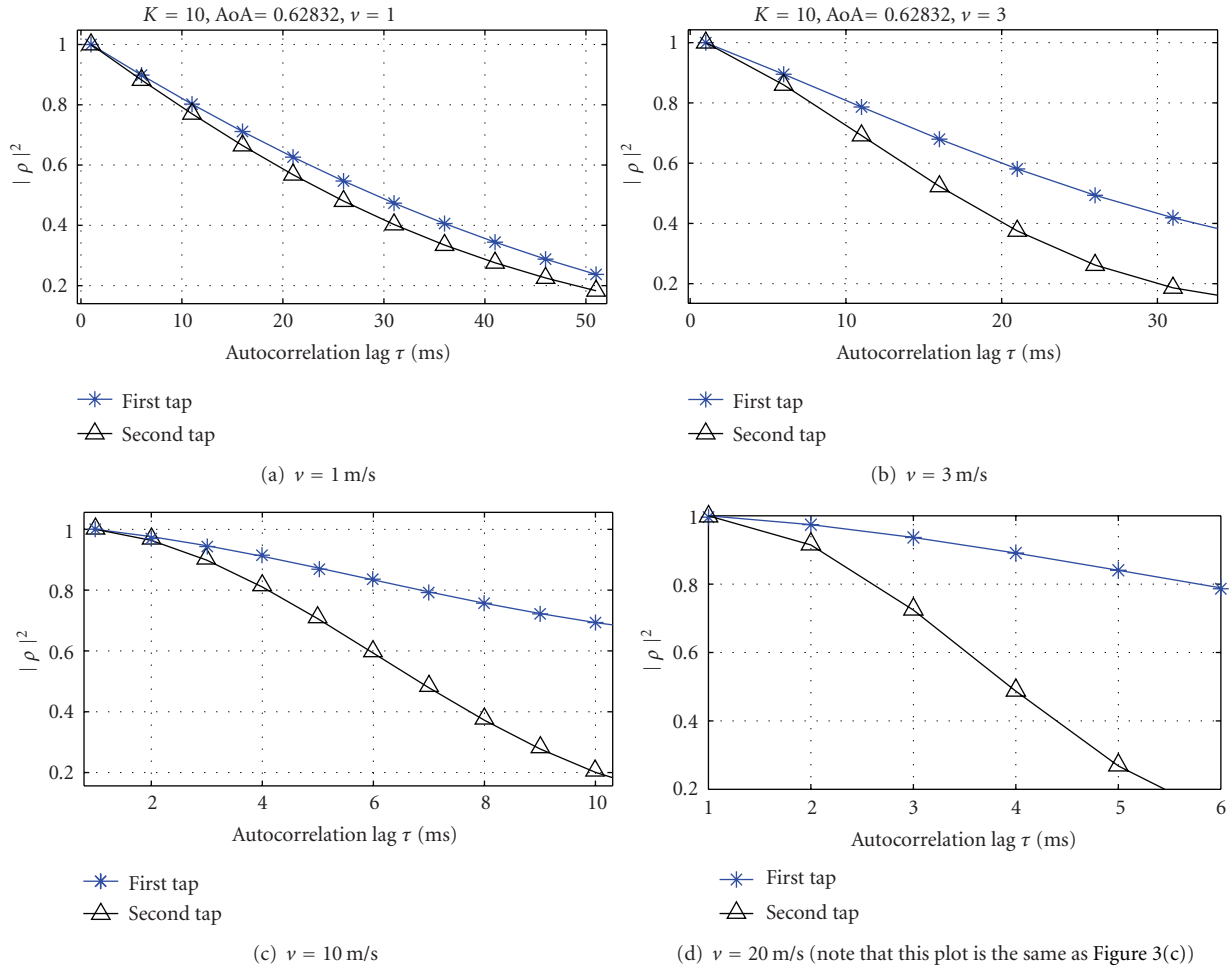

Figure 5: Squared-envelope of the autocorrelations of the first and second taps for common parameters $\theta_0^{(0)} = \pi/5$, $K_0 = 10$, and the set of $\{\nu\}$.

settings and sets are maintained except for K_0. In addition to the one presented in Table 1, two more values, namely, $K_{\text{new}} = \{0.5, 2\}$, are added to better see the impact when $K_0 < 3$. As can be seen from Figure 6, as soon as the power of specular component dominates, in other words when $K_0 \geq 1$, there are still cases that allow one to identify LOS even though $K_0 < 3$. This implies that LOS identification is statistically possible for even $1 \leq K_0 < 3$ in some practical scenarios, although Proposition 1 provides a universal bound for K_0. Furthermore, increase in ν causes this probability to drop even below 0.05 for time-varying specular components, namely, when $\theta_0^{(0)} \neq \pi/2$. This probability increases for $K_0 < 3$ with increasing ν and $\theta_0^{(0)} = \pi/2$. This stems from (8), since $\theta_0^{(0)} = \pi/2$ makes the $\cos(\cdot)$ term depend only on $\Psi(\Delta t)$. Because $\cos(\Psi(\Delta t)) < 1$ when $\Re(\rho_{d_k}(\Delta t)) < |\rho_{d_k}(\Delta t)|$, the inequality $|\rho_{h_0}(\Delta t)| < |\rho_{h_{\bar{k}}}(\Delta t)|$ holds for some $\Delta t = \Delta t_1$. Also, $\nu \to \infty$ implies $\Delta t_1 \to 0$. Therefore, as ν increases, by the time $|\rho_{h_{\bar{k}}}(\cdot)|$ reaches its coherence time at Δt_1, $\Re(\rho_{d_k}(\Delta t))$ decreases faster and causes $\cos(\Psi(\Delta t)) < 1$ leading to lower values of $|\rho_{h_0}(\Delta t_1)|$ compared to $|\rho_{h_{\bar{k}}}(\Delta t_1)|$.

Up until this point, Case 1 is considered in simulations. However, as discussed earlier, underlying process in each channel might be different. In order to test the method proposed for Case 2 scenarios, two diferent Doppler spectra for underlying processes are considered: Jakes' and GAUS1 type. GAUS1 type Doppler spectrum is given by [31]

$$P(f) = G\left(A, -0.8\left(\frac{\omega_D}{2\pi}\right), 0.05\left(\frac{\omega_D}{2\pi}\right)\right) + G\left(0.1A, 0.4\left(\frac{\omega_D}{2\pi}\right), 0.1\left(\frac{\omega_D}{2\pi}\right)\right), \tag{25}$$

where

$$G(A, f_1, f_2) = A\ \exp\left(-\frac{(f - f_1)^2}{2f_2^2}\right), \tag{26}$$

and A is the normalization constant. In Case 2 scenarios, it is assumed that the underlying process of the first tap to be of Jakes' type, whereas that of the second tap is GAUS1 based on (25) and (26).(Note that this simulation setup resembles COST 207 typical urban channel model [31]. The difference is that in COST 207 typical urban channel model, GAUS1 is observed in the third tap, not in the second tap.

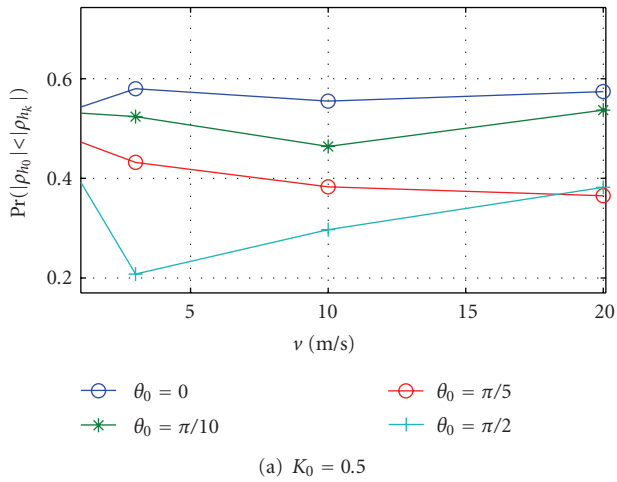

(a) $K_0 = 0.5$

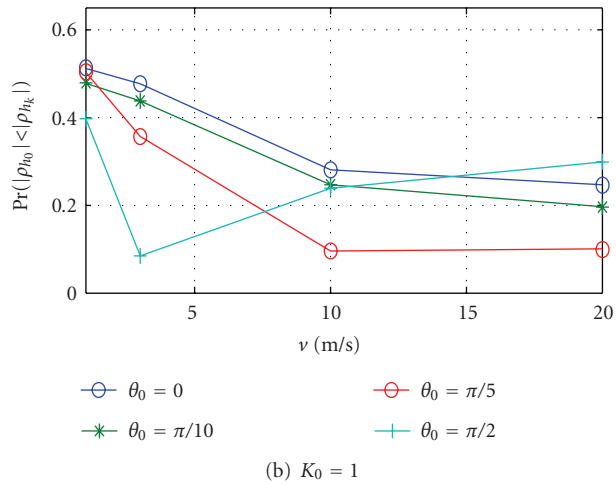

(b) $K_0 = 1$

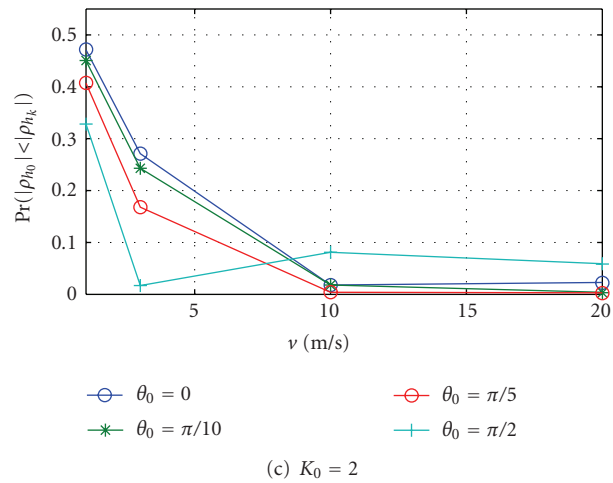

(c) $K_0 = 2$

FIGURE 6: The probability of $|\rho_{h_s}(\Delta t_1)|^2 < \rho_{h_d}(\Delta t_1)|^2$ versus the mobile speed for different AoAs under the assumption of Case 1 along with underlying process (I).

Besides, the first tap consists only of the underlying process of Jakes' type without a LOS component. Since the original COST 207 typical urban channel model is already considered in Case 1, Case 2 simulations are established by modifying

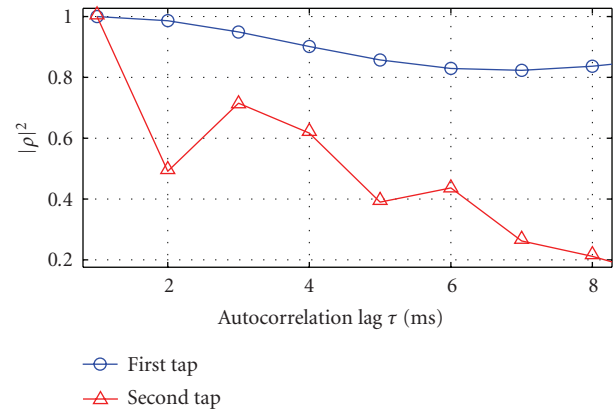

FIGURE 7: An example realization of Case 2 for the common parameter set defined in Section 3. The underlying processes are of Jakes' and of GAUS1 type for the first and second taps, respectively.

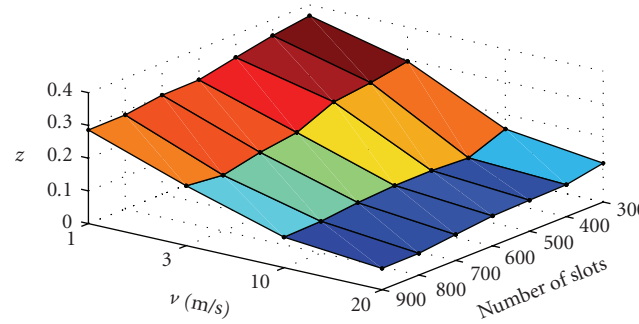

FIGURE 8: The threshold z values, which keep the false alarm rate $\Pr(\text{LOS}|(\mathcal{T} = \text{NLOS}))$ at 0.05 confidence level, for different number of slots and v values.

COST 207 typical urban channel model by providing a LOS component to the first tap and using GAUS1 type as the underlying process for the second tap.) Figure 7 shows the result for the common parameter set defined previously. As can be seen, when the second tap reaches its coherence time ($|\rho_{h_{\bar{k}}}(\Delta t_1)|^2 = 0.25$), there is a significant difference between $|\rho_{h_0}(\Delta t_1)|^2$ and $|\rho_{h_{\bar{k}}}(\Delta t_1)|^2$, in accordance with Proposition 1 regardless of having different underlying processes.

As stated in Section 2.3, due to physical limitations, receivers use estimations of autocorrelation coefficients by taking limited number of slots (samples) into consideration. Therefore, the identification process is established via a nonnegative threshold z. It must be stated that z depends mainly on number of slots, K_0, speed (v), and SNR. Therefore, it is very difficult, if not impossible, to obtain a closed-form solution to the problem of selection z. In this study, z values are obtained using numerical evaluation by keeping the false alarm rate, namely, $\Pr(\text{LOS}|(\mathcal{T} = \text{NLOS}))$, at 0.05 for each specific number of slots and v value along with the assumption of perfect channel estimation, where $\Pr(\mathcal{X}|\mathcal{Y})$ denotes the probability of event $\mathcal{X}$, given event $\mathcal{Y}$. As shown in Figure 8, desired z values form a surface whose value decreases with the increase of number of slots and v. The threshold z can be adjusted accordingly in case

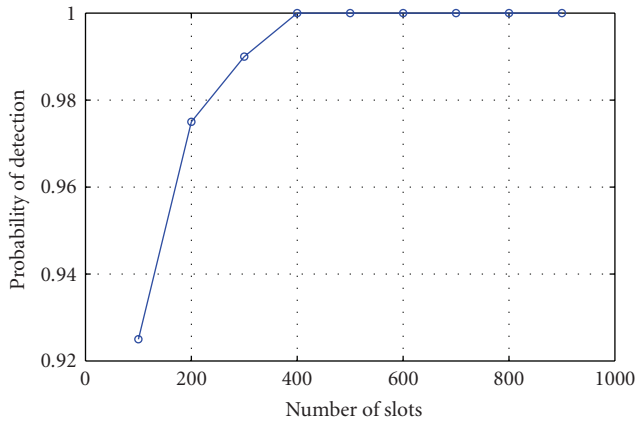

Figure 9: Probability of detection versus number of slots (N_{SLOT}) for $K_0 = 10$, $v = 20$ m/s, and SNR = 10 dB.

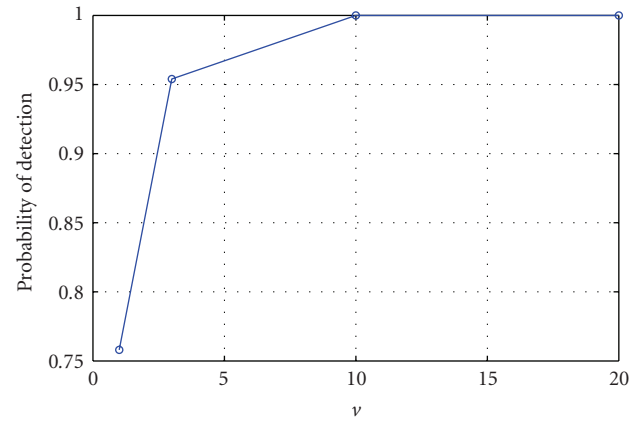

Figure 11: Probability of detection versus v for SNR = 10 dB, $N_{SLOT} = 500$, and $K_0 = 10$.

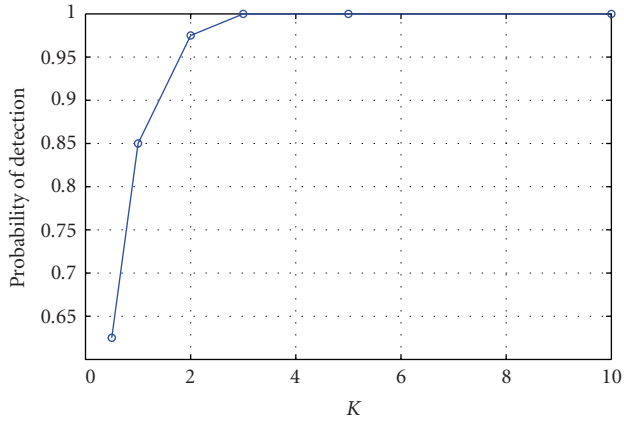

Figure 10: Probability of detection versus K_0 for $v = 20$ m/s, SNR = 10dB, and $N_{SLOT} = 500$.

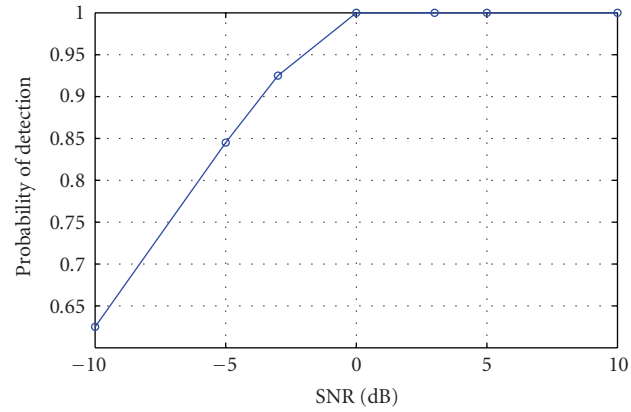

Figure 12: Probability of detection versus SNR for $N_{SLOT} = 500$, $K_0 = 10$, and $v = 20$ m/s.

the receiver knows the number of observation slots and/or v. In the simulations of category (ii), as will be discussed subsequently, for comparison purposes, f_s is 1.5 KHz. The number of slots in the general parameter subset is chosen as 500 and v is assumed to be unknown. Based on the results shown in Figure 8, the minimum of z values, namely, $z = 0.1$, is chosen as the threshold and performance of the method proposed is evaluated based on this value.

In category (ii), the channel estimation errors are introduced into the identification process. In order to test the performance of the method proposed, least-squares channel estimation is employed by keeping SNR = 10 dB along with the common parameter subset. The results are shown in Figures 9–12. It is seen from Figure 9 that as N_{SLOT} increases, the detection rate increases, since the estimation of the autocorrelation coefficients becomes more reliable. The detection rate becomes unity for $N_{SLOT} \geq 400$. In Figure 10, the impact of K_0 value can be observed. For the general parameter subset, even lower K_0 values can be detected. In order to investigate the impact of v, Figure 11 can be examined. In accordance with the discussion about the results presented in Figure 5, when $v \to 0$, the difference between the estimates of the autocorrelation coefficients of the taps cannot be distinguished; therefore, the detection rate is degraded. Figure 12 shows the impact of SNR on channel estimation and therefore identification process. For the values given in the parameter subset, it is seen that even for relatively low SNR values, the proposed method performs well.

Although the method proposed is based on the autocorrelation coefficient estimates of the channel taps, its performance in identification of LOS can be compared with those of which consider practical cases such as presented in [18]. According to [18], the method based on the comparison of distribution of the channel amplitudes reaches the certainty about identification of LOS after $N_{SLOT} = 880$ under a relatively fast fading channel with $v = 22.22$ m/s and $K_0 \approx 35.45$ (15.5 dB). With the same v and $K_0 \approx 31.62$ (15 dB), again in [18], the modified version of the previous algorithm reaches the certainty after $N_{SLOT} = 500$. The method proposed reaches the certainty about the identification at $N_{SLOT} = 300$ for a weaker specular component ($K_0 = 10$ dB) and a lower speed value ($v = 20$ m/s) via calculating the autocorrelation coefficients and a threshold value z, as shown

in Figure 9. Moreover, in simulations, it is shown that for such higher v values, the identification can be established very easily for even lower K_0 values ($K_0 = 2 = 1.58\,\text{dB}$). Note that the method proposed requires neither noise level estimation nor very long observation times. Apart from that, distribution comparison based approaches collect the channel estimations and rely on the estimation of Ricean factor in addition to distribution comparison operation. However, the method proposed solely needs the channel estimation and a threshold z, which can be fixed or changed adaptively depending on the capability of the receiver. The method proposed does not need to estimate the Ricean factor either.

4. CONCLUDING REMARKS

LOS/NLOS is one of the very important radio propagation channel parameters. Identification of LOS helps adaptive and cognitive wireless systems to perform better from the perspective of both radio transmission and wireless applications. In this study, it is proven that in time-varying, frequency selective radio channels, based on the assumption that perfect channel estimation is available, autocorrelation coefficient of the first tap is always greater than those of subsequent taps ($\bar{k}$) when any one of the subsequent taps reaches its coherence time while $K_0 > 3$. Regarding this fact, a method, which is based on the comparison of the autocorrelation coefficients of the channel taps and a concept named "underlying process," is developed to identify LOS. Simulation results are presented for both theoretical and practical cases in which perfect channel estimations are not available and different Doppler spectra are considered.

Even though this study assumes that $M_k \geq 1$, it does not require $M_k \to \infty$. However, when UWB channels are considered, due to increased time resolution (or equivalently very large transmission bandwidth), number of resolvable paths increases, which might remove the concept of underlying process by having $M_k = 0$. In these cases, the proposed method might not be sufficient to analyze LOS with the way that is mentioned previously and illustrated in Figure 1. Nonetheless, it is possible to take advantage of increased time resolution by considering the frequency resolution of each path one by one [32, 33]. It is reported in [32, 33] that, with a very fine time resolution as in UWB transmission, "path history" can be extracted from the frequency dependence of each path. Since the LOS path does not have frequency dependence [33], "path history" can be used in identifying LOS in UWB cases as well.

REFERENCES

[1] Federal Communications Commission, "Millimeter wave propagation: spectrum management implications," Federal Communications Commission, Office of Engineering and Technology Bulletin no. 70, New Technology Development Division, Washington, DC, USA, July 1997.

[2] A. F. Molisch, "Ultrawideband propagation channels-theory, measurement, and modeling," *IEEE Transactions on Vehicular Technology*, vol. 54, no. 5, pp. 1528–1545, 2005.

[3] J. Kunisch and J. Pamp, "Measurement results and modeling aspects for the UWB radio channel," in *Proceedings of IEEE Conference on Ultra Wideband Systems and Technologies (UWBST '02)*, pp. 19–23, Baltimore, Md, USA, May 2002.

[4] A. Durantini, W. Ciccognani, and D. Cassioli, "UWB propagation measurements by PN-sequence channel sounding," in *Proceedings of IEEE International Conference on Communications (ICC '04)*, vol. 6, pp. 3414–3418, Paris, France, June 2004.

[5] Federal Communications Commission, "Revision of the commissions rules to ensure compatibility with enhanced 911 emergency calling systems," CC Docket no. 94-102, RM-8143, FCC, Washington, DC, USA, December 1997, http://www.fcc.gov/Bureaus/Wireless/Orders/1997/da972530.pdf.

[6] C. Botteron, A. Høst-Madsen, and M. Fattouche, "Effects of system and environment parameters on the performance of network-based mobile station position estimators," *IEEE Transactions on Vehicular Technology*, vol. 53, no. 1, pp. 163–180, 2004.

[7] M. P. Wylie and J. Holtzman, "The non-line of sight problem in mobile location estimation," in *Proceedings of the 5th IEEE International Conference on Universal Personal Communications (ICUPC '96)*, vol. 2, pp. 827–831, Cambridge, Mass, USA, September-October 1996.

[8] S. Gezici, H. Kobayashi, and H. V. Poor, "Non-parametric non-line-of-sight identification," in *Proceedings of the IEEE 58th Vehicular Technology Conference (VTC '03)*, vol. 4, pp. 2544–2548, Orlando, Fla, USA, October 2003.

[9] Y.-C. Tseng, S.-L. Wu, W.-H. Liao, and C.-M. Chao, "Location awareness in ad hoc wireless mobile networks," *Computer*, vol. 34, no. 6, pp. 46–52, 2001.

[10] J. Mitola III, "Cognitive INFOSEC," in *Proceedings of IEEE MTT-S International Microwave Symposium Digest*, vol. 2, pp. 1051–1054, Philadelphia, Pa, USA, June 2003.

[11] S. Yarkan and H. Arslan, "Identification of LOS and NLOS for wireless transmission," in *Proceedings of IEEE Cognitive Radio Oriented Wireless Networks and Communications (CROWNCOM '06)*, vol. 1, pp. 1–5, Mykonos Island, Greece, June 2006.

[12] S. Yarkan and H. Arslan, "Exploiting location awareness toward improved wireless system design in cognitive radio," *IEEE Communications Magazine*, vol. 46, no. 1, pp. 128–136, 2008.

[13] H. Celebi and H. Arslan, "Cognitive positioning systems," *IEEE Transactions on Wireless Communications*, vol. 6, no. 12, pp. 4475–4483, 2007.

[14] J. Vidal and R. E. Játiva, "First arriving path detection for subscriber location in mobile communication systems," in *Proceedings of IEEE International Conference on Acoustics, Speech and Signal Processing (ICASSP '02)*, vol. 3, pp. 2733–2736, Orlando, Fla, USA, May 2002.

[15] J. Borras, P. Hatrack, and N. B. Mandayam, "Decision theoretic framework for NLOS identification," in *Proceedings of the 48th IEEE Vehicular Technology Conference (VTC '98)*, vol. 2, pp. 1583–1587, Ottawa, Canada, May 1998.

[16] S. Venkatraman and J. Caffery Jr., "Statistical approach to non-line-of-sight BS identification," in *Proceedings of the 5th International Symposium on Wireless Personal Multimedia Communications*, vol. 1, pp. 296–300, Honolulu, Hawaii, USA, October 2002.

[17] M. Feder and N. Merhav, "Universal composite hypothesis testing: a competitive minimax approach," *IEEE Transactions on Information Theory*, vol. 48, no. 6, pp. 1504–1517, 2002.

[18] A. Lakhzouri, E. S. Lohan, R. Hamila, and M. Rentors, "Extended Kalman filter channel estimation for line-of-sight detection in WCDMA mobile positioning," *EURASIP Journal on Applied Signal Processing*, vol. 2003, no. 13, pp. 1268–1278, 2003.

[19] S. Al-Jazzar and J. Caffery Jr., "New algorithms for NLOS identification," in *Proceedings of the 14th IST Mobile and Wireless Communications Summit*, Dresden, Germany, June 2005.

[20] R. A. Iltis, "Joint estimation of PN code delay and multipath using the extended Kalman filter," *IEEE Transactions on Communications*, vol. 38, no. 10, pp. 1677–1685, 1990.

[21] R. A. Iltis and L. Mailaender, "An adaptive multiuser detector with joint amplitude and delay estimation," *IEEE Journal on Selected Areas in Communications*, vol. 12, no. 5, pp. 774–785, 1994.

[22] K. J. Kim and R. A. Iltis, "Joint detection and channel estimation algorithms for QS-CDMA signals over time-varying channels," *IEEE Transactions on Communications*, vol. 50, no. 5, pp. 845–855, 2002.

[23] A. Lakhzouri, E. S. Lohan, R. Hamila, and M. Renfors, "Solving closely-spaced multipaths via extended Kalman filter in WCDMA downlink receivers," in *Proceedings of the 5th European Personal Mobile Communications Conference*, pp. 271–275, Glasgow, UK, April 2003.

[24] A. Lakhzouri, E.-S. Lohan, and M. Renfors, "Estimation of closely-spaced paths via particle filters for WCDMA positioning," in *Proceedings of the 1st International Symposium on Control, Communications and Signal Processing (ISCCSP '04)*, pp. 791–794, Hammamet, Tunisia, March 2004.

[25] T. S. Rappaport, *Wireless Communications: Principles and Practice*, Prentice Hall Communications Engineering and Emerging Technologies Series, Prentice-Hall, New Jersey, NJ, USA, 2nd edition, 2002.

[26] C. Tepedelenlioglu and G. B. Giannakis, "On velocity estimation and correlation properties of narrow-band mobile communication channels," *IEEE Transactions on Vehicular Technology*, vol. 50, no. 4, pp. 1039–1052, 2001.

[27] G. L. Turin, F. D. Clapp, T. L. Johnston, S. B. Fine, and D. Lavry, "A statistical model of urban multipath propagation," *IEEE Transactions on Vehicular Technology*, vol. 21, no. 1, pp. 1–9, 1972.

[28] H. Suzuki, "Statistical model for urban radio propagation," *IEEE Transactions on Communications*, vol. 25, no. 7, pp. 673–680, 1977.

[29] X. Zhao, J. Kivinen, P. Vainikainen, and K. Skog, "Characterization of Doppler spectra for mobile communications at 5.3 GHz," *IEEE Transactions on Vehicular Technology*, vol. 52, no. 1, pp. 14–23, 2003.

[30] ITU-Radiocommunication, "Guidelines for evaluation of radio transmission technologies for IMT-2000," Tech. Rep. ITU-R M.1225, International Telecommunication Union, Geneva, Switzerland, 1997.

[31] COST 207 Management Committee, "COST 207: digital land mobile radio communications," Commission of the European Communities, Final Report, December 1989.

[32] R. C. Qiu and I.-T. Lu, "Wideband wireless multipath channel modeling with path frequency dependence," in *Proceedings of IEEE International Conference on Communications, Converging Technologies for Tomorrow's Applications (ICC '96)*, vol. 1, pp. 277–281, Dallas, Tex, USA, June 1996.

[33] R. C. Qiu and I.-T. Lu, "Multipath resolving with frequency dependence for wide-band wireless channel modeling," *IEEE Transactions on Vehicular Technology*, vol. 48, no. 1, pp. 273–285, 1999.